Relativistic convergent close-coupling method: Calculation of electron scattering from hydrogenlike ions

Christopher J. Bostock,* Dmitry V. Fursa, and Igor Bray
ARC Centre for Antimatter-Matter Studies, Curtin University, GPO Box U1987, Perth, Western Australia 6845, Australia
(Received 17 June 2009; published 18 November 2009)

We report on the extension of the recently formulated relativistic convergent close-coupling (RCCC) method to include the Breit and Møller interactions. The inclusion of these relativistic effects ensures that the RCCC method is now capable of calculating electron scattering excitation and ionization cross sections for highly charged ions. We have calculated the polarization of the Lyman-α_1 x-ray line emitted by hydrogenlike Ti^{21+}, Ar^{17+}, and Fe^{25+} ions excited by electron impact. We find that account of Breit relativistic corrections is important to resolve the discrepancy between experiment and theoretical calculations. For the much heavier hydrogenlike U^{91+} ion where the Møller interaction becomes important we present the estimate of the polarization of the Lyman-α_1 x-ray line and performed a calculation of the total ionization cross section.

DOI: 10.1103/PhysRevA.80.052708 PACS number(s): 34.80.Bm, 34.80.Nz

I. INTRODUCTION

The recent development of the relativistic convergent close-coupling (RCCC) method [1,2] enables it to be applied to electron scattering from heavy targets where relativistic effects are important in both the target structure and scattering dynamics. We report on the further extension of the RCCC method to include the Breit [3–5] and Møller [6] interactions. The Breit interaction is a relativistic correction that is added to the Coulomb potential and is valid in the limit of low energy transfer between the two interacting electrons. The Møller interaction incorporates the Coulomb potential and is obtained as a lowest order QED interaction that is valid for arbitrary energy transfer between electrons.

Bethe and Salpeter [7] and Greiner [8] highlight that the Breit interaction is strictly only applicable in the context of perturbation theory and its use as an interaction potential in the Dirac equation can lead to the wrong results due to the mixing of positive and negative energy states. Sucher [9] has shown that these problems can be rectified with the use of positive energy projection operators in the interaction terms; this constitutes working in the no-virtual-pair approximation. The RCCC method is nonperturbative and relies on solving a set of coupled relativistic Lippmann-Schwinger equations derived from the Dirac equation. We, therefore, adopt the no-virtual-pair approximation in order to include the Breit and Møller interactions in the RCCC formalism.

Electron impact excitation cross sections for highly charged hydrogenlike targets have been calculated by Walker [10], Moores and Pindzola [11], and Fontes *et al.* [12] using relativistic perturbative first-order methods that compared Coulomb, Breit, and Møller interactions in the calculations. Similar first-order calculations that investigate the effects of the Breit and Møller interaction in electron impact total ionization cross sections for a range of hydrogenlike ions have been performed by Pindzola *et al.* [13,14], Moores and Reed [15,16], and Fontes *et al.* [17,18].

These calculations and associated development of computer codes have been done to a large degree in response to series of an electron-beam ion trap (EBIT) experiments (see [19] for a recent review) that investigated many fundamental processes involving highly charged ions excited by electron beams. For example, the experiment of Marrs *et al.* [20] for the 1*s* total ionization cross section of U^{91+} can be explained by theory only if the Møller interaction is used instead of the Coulomb interaction, with the latter underestimating the experiment by nearly 50%.

In addition to measurements of line intensities in EBIT experiments that lead to determination of various cross sections there have been numerous performed measurements of line polarizations. Such measurements play an important role in plasma diagnostics [21] and serve as sensitive tests of theoretical methods. In particular, Nakamura *et al.* [22] have demonstrated that there is a systematic discrepancy between measured polarization and results of fully relativistic distorted-wave calculations [23] for the hydrogenlike Ti^{21+} ion Lyman-α_1 x-ray line. Similar discrepancy has been found by Robbins *et al.* [24] for the hydrogenlike Ar^{17+} and Fe^{25+} ions. We will demonstrate in this paper that account of the Breit relativistic corrections is required to achieve agreement with experiment.

This paper is organized as follows: Sec. II contains an overview of the RCCC method, and the following Sec. III describes the inclusion of the Breit and Møller interactions. Following this, in Sec. IV we present results of our calculations for the polarization of the Lyman-α_1 x-ray line emitted by hydrogenlike Ti^{21+}, Ar^{17+}, and Fe^{25+} ions excited by electron impact. Similar calculations have also been performed for the much heavier hydrogenlike U^{91+} ion for which the total ionization cross section is also presented and compared with previous first-order perturbative calculations and experiment.

II. RCCC METHOD

The RCCC method has two main parts: first the structure of the target atom or ion is calculated, and then the relativistic Lippmann-Schwinger equation for the scattering problem is solved in momentum space. The RCCC method is

*c.bostock@curtin.edu.au

discussed in detail by Fursa *et al.* [2] and only the main features of the theory are highlighted here.

A. Relativistic target structure

The relativistic wave function $\phi(\boldsymbol{r})$ for the target electron in a hydrogenlike target is described by the Dirac equation

$$H_{\mathrm{T}}\phi(\boldsymbol{r}) = (c\boldsymbol{\alpha}\cdot\boldsymbol{p} + \beta m_0 c^2 + V_{\mathrm{T}})\phi(\boldsymbol{r}) = \epsilon\phi(\boldsymbol{r}), \tag{1}$$

where α and β are the Dirac matrices, c is the speed of light, m_0 is the electron mass, and $\boldsymbol{p}$ is the momentum operator. We use atomic units and take $m_0=\hbar=1$ and $c=137.036$. We assume a model of a point nucleus with infinite mass. For a central potential V_{T} the solutions of Dirac equation (1) are characterized by the relativistic quantum number κ and are given by a four-component spinor [25]

$$\phi_{\kappa m}(\boldsymbol{r}) = \frac{1}{r}\begin{pmatrix} \phi_\kappa^{\mathrm{L}}(r)\chi_{\kappa m} \\ i\phi_\kappa^{\mathrm{S}}(r)\chi_{-\kappa m}\end{pmatrix}. \tag{2}$$

Here $\phi_\kappa^{\mathrm{L}}(r)$ and $\phi_\kappa^{\mathrm{S}}(r)$ are the large and small components of the radial wave function, $\chi_{\kappa m}$ is a two-component coupled spin-orbit function, and m is the magnetic quantum number. The relativistic quantum number κ is related to the total angular momentum j and parity $\pi=(-1)^l$ of the orbital via

$$j = |\kappa| - \frac{1}{2}, \tag{3}$$

$$l = \begin{cases} \kappa, & \kappa > 0, \\ -\kappa - 1 & \kappa < 0. \end{cases} \tag{4}$$

The Dirac Hamiltonian in Eq. (1) is diagonalized using a Dirac L-spinor basis [26]. Dirac L spinors form a Sturmian basis which spans both positive energy and negative energy parts of the Dirac equation spectrum. The target atom wave function $\phi_{\kappa m}(\mathbf{r})$ is sought as an expansion

$$\phi_{\kappa m}(\boldsymbol{r}) = \frac{1}{r}\begin{pmatrix} \phi_\kappa^{\mathrm{L}}(r)\chi_{\kappa m} \\ i\phi_\kappa^{\mathrm{S}}(r)\chi_{-\kappa m}\end{pmatrix} = \frac{1}{r}\begin{pmatrix} \sum_{n_r} C_{n_r}^{\mathrm{L}} f_{n_r\kappa}^{\mathrm{L}}(r)\chi_{\kappa m} \\ i\sum_{n_r} C_{n_r}^{\mathrm{S}} f_{n_r\kappa}^{\mathrm{S}}(r)\chi_{-\kappa m}\end{pmatrix}. \tag{5}$$

Here $C_{n_r}^{\mathrm{L}}$ and $C_{n_r}^{\mathrm{S}}$ are expansion coefficients, and $f_{n_r\kappa}^{\mathrm{L}}(r)$ and $f_{n_r\kappa}^{\mathrm{S}}(r)$ are Dirac L spinors. As described by Fursa *et al.* [2], expansion (5) is substituted into the Dirac equation, Eq. (1), allowing the target Hamiltonian to be diagonalized to obtain the target wave functions and energy levels. In order to stay within the no-virtual-pair approximation we retain only positive total energy solutions obtained from the diagonalization. Excellent agreement is found when the hydrogenlike target energy levels and wave functions generated with this procedure are checked against the relativistic analytic solutions [27], even for Z as high as 100.

B. Relativistic scattering formalism

The Dirac Hamiltonian for the total scattering system consisting of projectile and hydrogenlike target electron is given by

$$H = H_1 + H_2 + V_{12}, \tag{6}$$

where H_1 refers to the projectile Hamiltonian and H_2 refers to the target electron Hamiltonian. In each case

$$H_i = K_i + V_i = K_i + Z/r_i, \tag{7}$$

where K_i is the free Dirac Hamiltonian and Z is the charge of the nucleus. V_{12} in Eq. (6) is the electron-electron potential which is either Coulomb, Coulomb+Breit, or the Møller interaction. These interactions will be discussed in the next section.

The total scattering wave function satisfies

$$(E - H)|\Psi_i^{(+)}\rangle = 0, \tag{8}$$

where the superscript (+) denotes incoming plane- or Coulomb-wave and outgoing spherical-wave boundary conditions and the initial target state is ϕ_i and projectile momentum is k_i.

We use the set of target states $\{\phi_n^N\}$ to perform a multichannel expansion of the total wave function,

$$|\Psi_i^{N(+)}\rangle = \frac{1}{2}(1 - P_{12})|\psi_i^{N(+)}\rangle = \frac{1}{2}(1 - P_{12})\sum_n |f_{n,i}^N \phi_n^N\rangle, \tag{9}$$

where N specifies the total number of states used, $f_{n,i}^N$ are channel functions, and P_{12} is the space exchange operator. The explicit antisymmetrization in Eq. (9) guarantees that the total wave function satisfies the Pauli exclusion principle.

For a hydrogenlike target ion with asymptotic charge $Z_{\mathrm{as}}=Z-1$ the asymptotic Hamiltonian of the scattering system is defined as

$$H_{\mathrm{as}} = K_1 - \frac{Z_{\mathrm{as}}}{r_1} + H_2. \tag{10}$$

The distorted waves used in the scattering formalism, $|\boldsymbol{k}^{(\pm)}, \mu, b\rangle$, are solutions of the one-electron Dirac equation

$$(\epsilon - H_{\mathrm{as}} - U)|\boldsymbol{k}^{(\pm)}, \mu, b\rangle = 0, \tag{11}$$

where U is an arbitrary short-ranged distorting potential, μ is the spin magnetic number, and b is the sign of energy, $\epsilon = \pm\epsilon_k = \pm c\sqrt{k^2+c^2}$, with the positive sign corresponding to electrons and the negative sign to positrons (negative energy electrons).

The formulation of the close-coupling equations has been discussed by Fursa *et al.* [2]. Briefly, a set of coupled momentum-space Lippmann-Schwinger equations for the T matrix is derived from Dirac equation (8) with the help of the Green's function G_{as} associated with the asymptotic Hamiltonian (10). Spectral decomposition of the Green's function G_{as} contains both positive and negative total energy terms. Negative energy terms correspond to closed channels and are excluded in the RCCC formulation which, therefore, is equivalent to the no-virtual-pair approximation. Upon partial-wave expansion we obtain a set of relativistic partial-wave Lippmann-Schwinger equations for the T matrix

$$T_{fi}^{\Pi J}(k_f\kappa_f,k_i\kappa_i) = V_{fi}^{\Pi J}(k_f\kappa_f,k_i\kappa_i) + \sum_n \sum_\kappa \sum \int k^2 dk \times \frac{V_{fn}^{\Pi J}(k_f\kappa_f,k\kappa) T_{ni}^{\Pi J}(k\kappa,k_i\kappa_i)}{E-\epsilon_n^N-\epsilon_{k'}+i0}, \quad (12)$$

with the notation as specified in [2]. The resulting form of the Lippmann-Schwinger equations is the same as for the nonrelativistic case and involves transitions between positive energy states only; however, they contain relativistic kinematics.

Upon solution of Lippmann-Schwinger equations (12) we use the obtained T matrix to define the scattering amplitude $F_{fi}^{\mu_f\mu_i}(\theta)$ in the collision frame (z axis is along the incident momentum of the projectile; θ is the angle between scattered electron momentum and z axis) for a transition from a state ϕ_i with parity π_i, angular momentum j_i, its projection m_i to a state ϕ_f with parity π_f, angular momentum j_f, its projection m_f as

$$F_{m_fm_i}^{\mu_f\mu_i}(\theta) = -\sum_{\kappa_f\kappa_i J\Pi} i^{L_i-L_f} e^{\eta_{\kappa_f}+\eta_{\kappa_i}} C_{L_fM_f,1/2\mu_f}^{jm_i} C_{L_i0,1/2\mu_i}^{j'\mu_i} C_{jm_j,j_fm_f}^{JM_J} \times C_{j'\mu_i,j_im_i}^{JM_J} Y_{L_f}^{M_f}(\boldsymbol{k}_f) \sqrt{\frac{2L_i+1}{4\pi}} T_{fi}^{\Pi J}(k_f\kappa_f,k_i\kappa_i), \quad (13)$$

where $m_j=m_i+\mu_i-m_f$ and $M_f=m_j-\mu_f$. The spin-averaged cross section describing transitions between magnetic sublevels is defined as

$$\sigma_{m_fm_i} = \frac{1}{2}\sum_{\mu_f\mu_i} |F_{m_fm_i}^{\mu_f\mu_i}(\theta)|^2. \quad (14)$$

Averaging over initial magnetic sublevels we obtain the cross section for excitation of a particular magnetic sublevel

$$\sigma_{m_f} = \frac{1}{2j_i+1}\sum_{m_i} \sigma_{m_fm_i}. \quad (15)$$

Summing over final magnetic sublevels we obtain the standard integrated cross section

$$\sigma_{fi} = \sum_{m_fm_i} \sigma_{m_fm_i}. \quad (16)$$

III. BREIT AND MØLLER INTERACTIONS

In 1929 Breit [3–5] used classical arguments to include relativistic corrections to the Coulomb potential in helium fine structure calculations. In the Coulomb gauge the Breit interaction is of the form

$$V_{12}^{\mathrm{B}} = \frac{e^2}{r_{12}}\left[-\boldsymbol{\alpha}_1\cdot\boldsymbol{\alpha}_2 + \frac{1}{2}(\boldsymbol{\alpha}_1\cdot\boldsymbol{p}_1\boldsymbol{\alpha}_2\cdot\boldsymbol{p}_2)r_{12}^2\right]. \quad (17)$$

In the above potential the first term on the right-hand side can be interpreted as a "magnetic" interaction between electron spins, and the second term on the right-hand side can be interpreted as a "retardation" term due to the finite propagation time of the interaction between the electrons.

Møller [6], in 1932, derived the relativistic Coulomb interaction for electron-electron scattering processes from quantum electrodynamics. In the Lorentz gauge the Møller interaction takes the form [8]

$$V_{12}^{\mathrm{M}} = \frac{e^2}{r_{12}}(1-\boldsymbol{\alpha}_1\cdot\boldsymbol{\alpha}_2)e^{iKr_{12}}, \quad (18)$$

where $K=|E-E'|/c$, and E and E' denote the initial and final energies of one of the electrons. The form of the interaction is different if the Coulomb gauge is used; however, Hata and Grant [28] have shown that the Lorentz and Coulomb gauge forms for the interaction have equivalent matrix elements provided the wave functions used are derived from a local potential, which pertains to the wave functions used in this work. The Møller interaction incorporates both the Coulomb interaction and all relativistic corrections, whereas the Breit interaction given by Eq. (17) must be added to the Coulomb potential. The Møller interaction depends on the energy transferred between the electrons and in the limit of low energy transfer it reduces to the Coulomb plus Breit interaction [8].

The matrix elements of the Coulomb, Breit, and Møller interactions have been given by Grant [29] and expressed in a convenient form for computation by Walker [10]. The calculation of the matrix elements of the Møller interaction,

$$\langle ABJM|\frac{e^2}{r_{12}}(1-\boldsymbol{\alpha}_1\cdot\boldsymbol{\alpha}_2)e^{iKr_{12}}|CDJ'M'\rangle, \quad (19)$$

requires the identity

$$\frac{e^{iKr_{12}}}{r_{12}} = iK\sum_{\nu=0}^{\infty}(2\nu+1)j_\nu(Kr_<)[n_\nu(Kr_>) - ij_\nu(Kr_>)]\boldsymbol{C}^\nu(1)\cdot\boldsymbol{C}^\nu(2), \quad (20)$$

where $j_\nu(Kr_<)$ and $n_\nu(Kr_>)$ are spherical Bessel and Neumann functions [30], and $r_<, r_>$ specify the lesser and greater of r_1 and r_2, respectively. For the on-shell matrix elements $K=|E_C-E_A|/c=|E_D-E_B|/c$. In performing full RCCC calculations we require off-shell V-matrix elements, and to obtain these we follow the method outlined by Hata and Grant [28],

$$V_{12}^{\mathrm{M}} = 1/2[V_{12}^{\mathrm{M}}(K_{AC}) + V_{12}^{\mathrm{M}}(K_{BD})], \quad (21)$$

where $K_{AC}=|E_C-E_A|/c$ and $K_{BD}=|E_D-E_B|/c$.

Fontes *et al.* [12] have performed calculations that show that the effect of dropping the imaginary part in Eq. (20) is negligible and is of the order of 2%–3% for $1s-2s$, $1s-2p_{1/2}$, and $1s-2p_{3/2}$ excitation cross sections for a very highly charged $Z=100$ hydrogenlike target. Thus, only the real part of the Møller interaction may then be used.

IV. RESULTS

We present in this section results of our calculations of electron scattering from hydrogenlike Ti^{21+}, Ar^{17+}, Fe^{25+}, and U^{91+} ions. The structure model for all considered ions was generated by diagonalizing the target Hamiltonian in a Dirac

L-spinor basis (see [2]) consisting of $17s$, $17p$, $17d$, $17f$, and $17g$ states using an exponential fall off parameter $\lambda=Z$ where Z is the nuclear charge. Such a model leads to the states up to principle quantum number $n=5$ laying in the bound-state spectrum with the rest providing square integrable discretization of the target continuum.

Close-coupling RCCC calculations have been performed across a wide energy range by solving Lippmann-Schwinger equation (12) for (i) Coulomb and then (ii) Coulomb+Breit interactions. We have found that the full RCCC results are generally in good agreement ($\approx 5\%$) for all considered target ions with first-order "Born-Oppenheimer" (BO) calculations where the exchange of projectile and target electrons is included but only the first term on the right-hand side in the set of Lippmann-Schwinger equations (12) is kept. Given the apparent lack of interchannel coupling we will normally present results for first-order BO calculations and give brief comments for the cases where interchannel coupling plays a more important role. In all results presented the term "Breit" implies Coulomb+Breit interactions incorporated together.

A. Polarization of the Lyman-α_1 line

Magnetic sublevel excitation cross sections of the $2p_{3/2}$ state from the ground $1s_{1/2}$ state given by Eq. (15) are required to determine the polarization of the $2p_{3/2} \rightarrow 1s_{1/2}$ line. These cross sections are related to the polarization by the following expression:

$$P = \frac{3(\sigma_{1/2} - \sigma_{3/2})}{3\sigma_{3/2} + 5\sigma_{1/2}}, \tag{22}$$

where σ_{m_f} is the cross section for excitation to a magnetic sublevel given by Eq. (15).

Cascades from the high-lying excited levels (up to $n=5$) to the $2p_{3/2}$ state can affect the polarization of the $2p_{3/2} \rightarrow 1s_{1/2}$ line. We will refer to the cross section and polarization obtained without account of cascades as direct and those obtained with account of cascades as apparent. We take into account the cascades by considering the contribution to the $2p_{3/2}$ state magnetic sublevel cross section σ_{m_f} from an upper lying state n with cross section σ_{m_n} to be

$$\sigma_{m_f}^{\mathrm{casc},m_n} = \sigma_{m_n} b(n,f) \langle j_f m_f 1q | j_n m_n \rangle^2, \tag{23}$$

where $\langle j_f m_f 1q | j_n m_n \rangle$ is a Clebsh-Gordan coefficient and $b(n,f)$ is the branching ratio for dipole radiative decay from the upper level n to the lower level f. By applying this formula to all possible radiative decay paths and summing over all bound states we obtain an estimate of the total cascade correction

$$\sigma_{m_f}^{\mathrm{app}} = \sigma_{m_f} + \sum_n \sum_{m_n} \sigma_{m_f}^{\mathrm{casc},m_n}. \tag{24}$$

The direct plus cascades values of magnetic sublevel $2p_{3/2}$ state (apparent) cross sections $\sigma_{m_f}^{\mathrm{app}}$ are then used in calculation of polarization via Eq. (22). This scheme has been used with good results in a number of our previous publications [31–33]. A more sophisticated account of cascades can be done via the collision-radiative kinetic model [34,35]. This model, however, reduces to our approach if all stepwise electron excitation and deexcitation processes are neglected which is a good approximation in the case of EBIT experiments due to the low ion density.

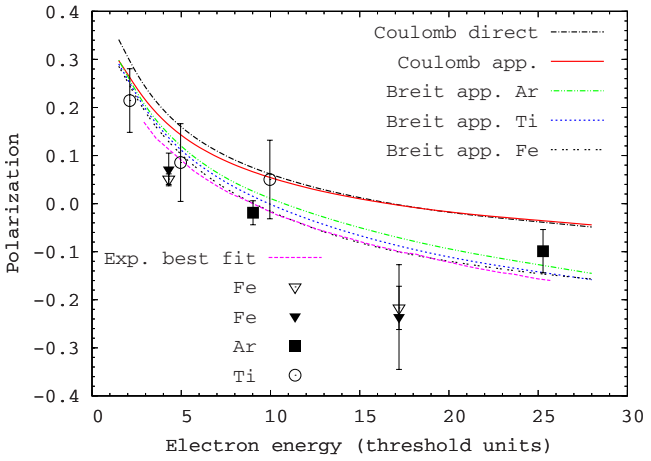

FIG. 1. (Color online) Polarization of Lyman-α_1 emission line of Ar^{17+}, Ti^{21+}, and Fe^{25+}. Present calculations are compared with experimental data of Nakamura *et al.* [22] and Robbins *et al.* [24]. Presented Coulomb potential calculations are for Ti^{21+} ion (results for Ar^{17+} and Fe^{25+} ions are practically the same). The two sets of experimental results for Fe^{25+} pertain to the two experiments outlined in [24].

In Fig. 1 and Table I we present results of our calculations for the polarization of Lyman-α_1 emission line of Ar^{17+}, Ti^{21+}, and Fe^{25+} ions. Our calculations for direct polarization (no cascade corrections) with Coulomb potential are in good agreement with previous Coulomb potential distorted-wave calculations of Reed and Chen [23] and results of distorted-wave code of Zhang *et al.* [36] reported by Robbins *et al.* [24]. Similarly to previous calculations we found little difference between the polarizations of the three considered ions when results are presented in threshold units. The cascades provide approximately equal contributions to each of the $m_f=3/2$ and $m_f=1/2$ magnetic sublevel cross sections, and the effect of the cascades on polarization of the Lyman-α_1 line proved to be minor. This can be seen in Fig. 1 by comparing Coulomb potential direct and apparent polarizations. We estimate that cascade corrections lead to about 10% depolarization of the radiation.

We find that the cascade effects are of similar magnitude for both Coulomb and Breit potential calculations. Hence, only cascade corrected (apparent) results are presented for the latter calculations. Our Breit potential calculations show substantial difference from the Coulomb potential calculations and are in very good agreement with the experimental results of Nakamura *et al.* [22] for Ti^{21+}, Robbins *et al.* [24] for Ar^{17+} and Fe^{25+} ions, and in particular with the line of best fit to experimental data as presented by Robbins *et al.* [24]. At low energies an account of channel coupling and in particular coupling to the ionization continuum has only a minor effect on the direct cross section and polarization; however, it reduces the effect of cascading and brings the direct and apparent cross sections closer together.

The difference between Coulomb potential and Breit potential calculations is greater at larger energies which is con-

TABLE I. Cascade corrected (apparent) and direct polarization results for Lyman-α_1 for Ar^{17+}, Ti^{21+}, and Fe^{25+} ions compared to experimental measurements of Nakamura *et al.* [22] for Ti^{21+}, and Robbins *et al.* [24] for Ar^{17+} and Fe^{25+}. The two sets of experimental results for Fe^{25+} pertain to the two experiments outlined in [24].

Energy (keV)		Coulomb	Breit	Experiment	
			Ar^{17+}		
30	App.	+0.063	+0.027	-0.019 ± 0.025	
	Dir.	+0.070	+0.031		
84	App.	−0.051	−0.128	-0.099 ± 0.045	
	Dir.	−0.056	−0.144		
			Ti^{21+}		
10.6	App.	+0.262	+0.250	$+0.214 \pm 0.066$	
	Dir.	+0.296	+0.283		
24.7	App.	+0.143	+0.113	$+0.085 \pm 0.081$	
	Dir.	+0.161	+0.127		
49.6	App.	+0.055	−0.0009	$+0.050 \pm 0.082$	
	Dir.	+0.062	−0.0003		
			Fe^{25+}		
30	App.	+0.165	+0.128	(a) $+0.071 \pm 0.034$	(b) $+0.051 \pm 0.011$
	Dir.	+0.186	+0.145		
120	App.	+0.0073	−0.102	(a) -0.236 ± 0.109	(b) -0.217 ± 0.045
	Dir.	+0.0095	−0.114		

sistent with expected increasing effect of relativistic corrections with the increase in incident electron energy. Similarly, at larger energies we can see the change in polarization with the change in nuclear charge (variation in polarization between Ar^{17+}, Ti^{21+}, and Fe^{25+} ions). We have also performed calculations using the Møller potential and found only minor differences from Breit potential calculations at large incident electron energies for these ions.

The effect of the Breit interaction and cascades on the $2p_{3/2}$ state integrated cross section is illustrated in Fig. 2 for the Ti^{21+} ion. We find that cascading plays a relatively larger role for cross sections compared to its effect on the line polarization, especially at lower energies. However, the relativistic corrections to the Coulomb interaction cannot be distinguished for these intermediately charged ions. In Fig. 3 we present direct magnetic sublevel cross sections for $2p_{3/2}$ state calculated with the Coulomb and Breit potentials. Account of Breit relativistic corrections leads to a slight increase in the cross sections, with the cross section for the $m=1/2$ sublevel being affected more than for the $m=3/2$ sublevel. It is this difference that is emphasized in the calculation of the polarization of Lyman-α_1 emission line and makes measurements of polarization a sensitive test of relativistic effects in electron-ion scattering.

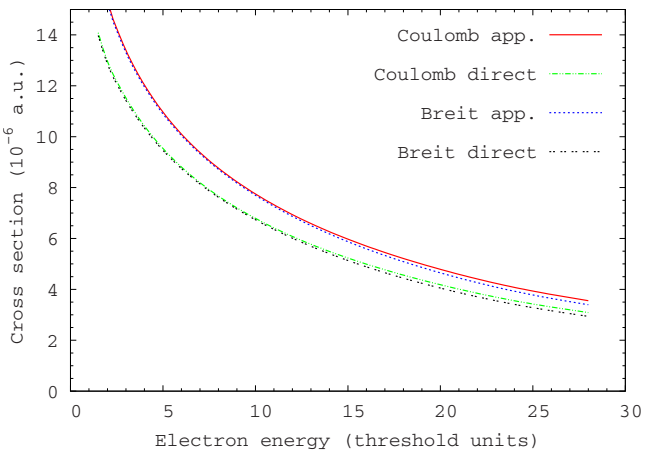

FIG. 2. (Color online) Direct and apparent cross sections for excitation of the $2p_{3/2}$ state of Ti^{21+}. Present calculations are described in text.

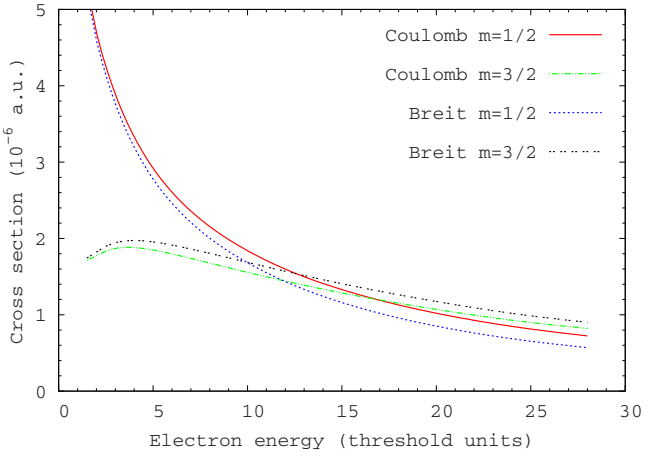

FIG. 3. (Color online) magnetic sublevel direct cross sections for excitation of the $2p_{3/2}$ state of Ti^{21+}. Present calculations are described in the text.

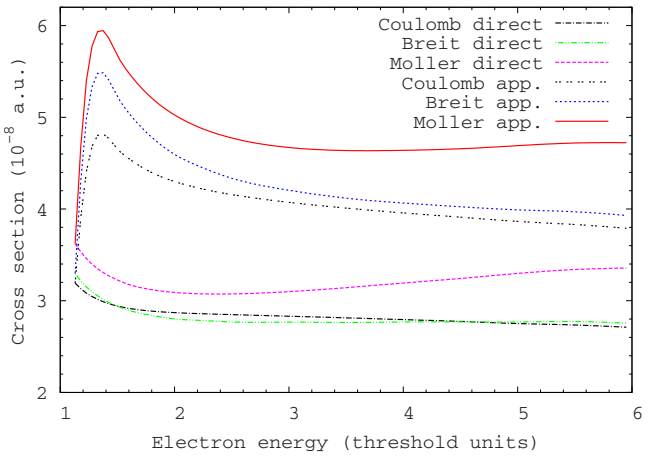

FIG. 4. (Color online) Direct and apparent cross sections for excitation of the $2p_{3/2}$ state of U^{91+}. Present calculations are described in the text.

Relativistic corrections to the Coulomb interaction become more important as the charge of an ion increases. It is, therefore, interesting to investigate the electron scattering from hydrogenlike U^{91+} ion. The EBIT experiment of Marrs *et al.* [20] concentrated on measurements of total ionization cross section (see next section). A new EBIT experiment at GSI Darmstadt is forthcoming [37] and is expected to determine the Lyman-α_1 line polarization.

In support of this experiment we have conducted a calculation of e-U^{91+} scattering. Direct and apparent cross sections for excitation of the $2p_{3/2}$ state are presented in Fig. 4. We find good agreement with previous calculations of $2s_{1/2}$, $2p_{1/2}$, and $2p_{3/2}$ direct cross sections by Moores and Pindzola [11] and Fontes *et al.* [12] performed with Coulomb, Breit, and Møller potentials. Account of Breit relativistic corrections does not change the cross section substantially while account of the Møller interaction leads to a much stronger effect. Cascade corrections proved to be very large ranging from about 50% at lower energies to 30% at larger energies.

In Fig. 5 we present our predictions for the polarization of the Lyman-α_1 emission line of U^{91+}. As expected an account

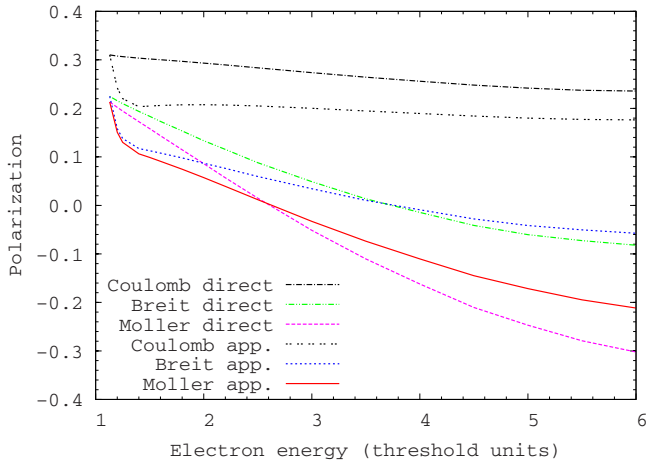

FIG. 5. (Color online) Polarization of Lyman-α_1 emission line of U^{91+}. Present calculations are described in the text.

of relativistic corrections leads to a large change in polarization. Calculations with the Coulomb potential lead to polarization that varies little across the considered energy range from one to six times the excitation threshold. Both Breit and Møller relativistic corrections lead to polarization that changes significantly more across the same energy range. At low energies the Breit and Møller potential results converge to the same polarization values, which is different to the Coulomb potential. At large energies the Breit and Møller potential results diverge with Møller potential results showing much larger variation across the energy range. Cascading leads to substantial depolarization of the radiation. Its effect is much larger for the U^{91+} ion than for the lower charged ions considered in this paper. Given such a large effect a more accurate account of cascading via the collision-radiative kinetic model [34,35] seems to be warranted. This will be investigated in the future. We note, however, that regardless of the accuracy the cascading is accounted for in present work our calculations predict a clear distinction between calculations of Lyman-α_1 emission line polarization with Coulomb, Breit, and Møller potentials. The difference between these calculations appears to be sufficiently large to be observed in experiment.

B. Ionization cross section of U^{91+}

In the RCCC method to obtain the total ionization cross section we sum over all the excitation cross sections that correspond to excitation of pseudostates above the ionization threshold

$$\sigma_{\text{ioniz}} = \sum_{f:0\le\epsilon_f\le E} \sigma_{fi}, \tag{25}$$

where ϵ_f is the energy of the pseudostate and E is the total energy of the system.

When the RCCC code is run in first-order mode the total ionization cross section is instead obtained using

$$\sigma^{\text{BO}}_{\text{ioniz}} = \sum_{f:0\le\epsilon_f\le E/2} \sigma^{\text{BO}}_{fi}, \tag{26}$$

where the sum only extends up to $E/2$. This is required in order to avoid double counting of pseudostates that represent the continuum. This method seems to be inconsistent with Eq. (25) employed in the full RCCC method; however, it has been demonstrated [38] that $\sigma_{fi}(\epsilon_f)\to 0$ for $\epsilon_f > E/2$ with an increasing number of states, N. That is, $\sigma_{fi}(\epsilon_f)$ converges to a step function as the number of states used in the calculation increases and this is a consequence of interchannel coupling in the RCCC method. The effect of double counting the pseudostates in first-order total ionization cross section calculations is demonstrated for the Coulomb interaction case in Fig. 6, where it can be seen that the U^{91+} total ionization cross section for the $1s$ electron is not in agreement with the full RCCC results if double counting occurs, whereas when double counting is avoided the first-order calculations are in excellent agreement with the full RCCC calculations.

We have performed first-order BO total ionization cross-section calculations for U^{91+} with (i) Coulomb and (ii) Møller interactions included and we found excellent agree-

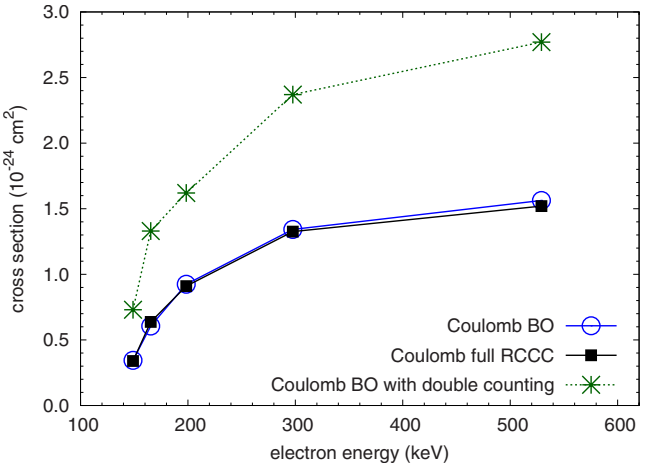

FIG. 6. (Color online) U^{91+} total ionization cross section for the 1*s* electron calculated with the Coulomb interaction. Full close-coupling (RCCC) results are compared to the first-order Born-Oppenheimer (BO) results obtained with and without account for double counting.

ment with the corresponding results of Fontes *et al.* [18], as shown in Fig. 7. In the RCCC method the continuum is modeled by pseudostates generated from an asymptotic nuclear charge of $Z-1$. This differs from the calculations of Fontes *et al.* [18] where the continuum states are generated from a nuclear charge Z. However, for a highly charged target with large Z the difference is apparently minimal.

We have also found that the effects of distortion of the target charge distribution [represented by the choice of U in Eq. (11)] were negligible. This can be readily understood by noting that the distorting potential U is only minor compared to the U^{91+} Coulomb potential.

The results presented in Fig. 7 include the exchange of projectile and target electrons. It has been highlighted by Moores and Reed [15] and Fontes *et al.* [17] that the account of the exchange of projectile and target electrons in the calculations of the U^{91+} 1*s* total ionization cross section leads to

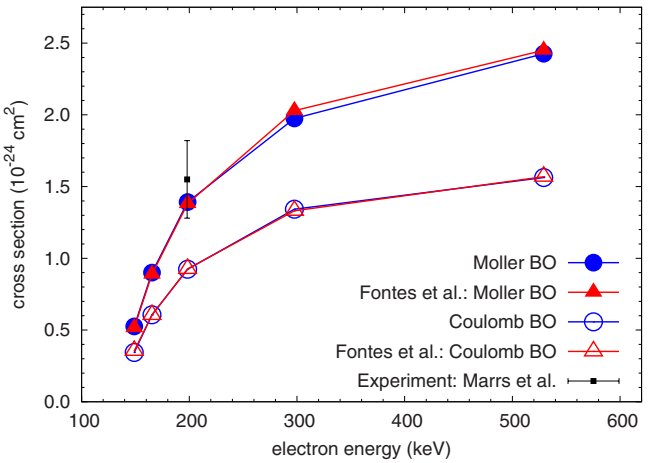

FIG. 7. (Color online) U^{91+} total ionization cross section for the 1*s* electron. Present results are compared with the first-order BO calculations of Fontes *et al.* [18] and the experimental results of Marrs *et al.* [20].

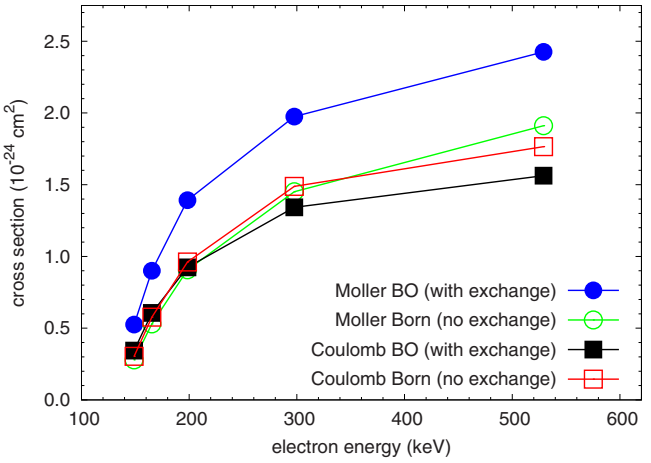

FIG. 8. (Color online) First-order U^{91+} total ionization cross-section calculations for the 1*s* electron illustrating the effects of the exchange of projectile and target electrons.

only minimal changes in the case of the Coulomb interaction, but has a significant effect in the case of the Breit and Møller interactions and is crucial in achieving agreement with experiment of Marrs *et al.* [20]. We indeed found this to be the case as illustrated in Fig. 8.

It is interesting to note that even though the account of the exchange leads to only a minor change in the U^{91+} 1*s* total ionization cross section for the Coulomb interaction, it does not mean that the exchange scattering is negligible. This is illustrated in Fig. 9 for the ionization spin asymmetries [39]. Large values of the ionization spin asymmetries indicate the importance of the exchange scattering not only for the Breit and Møller potentials but also for the Coulomb potential.

V. CONCLUSION

The recently formulated relativistic convergent close-coupling method has been extended to include the Breit and Møller interactions. The method has been applied to calculation of the polarization of the Lyman-α_1 line of Ti^{21+}, Ar^{17+},

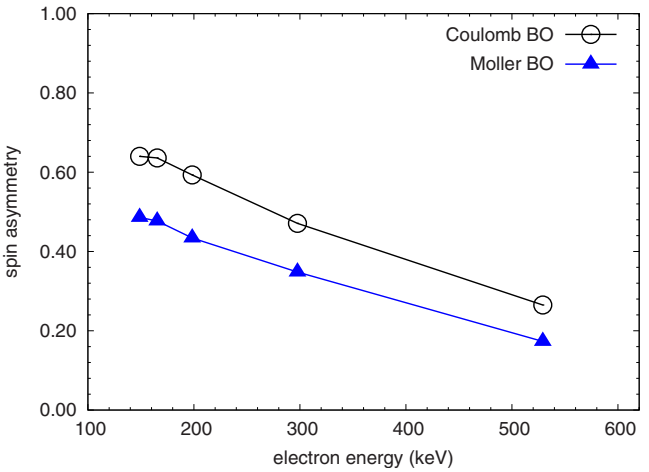

FIG. 9. (Color online) U^{91+} ionization spin asymmetries for the 1*s* electron.

and Fe^{25+} ions. We have shown that account of the Breit relativistic correction to the Coulomb interaction resolves the discrepancy between theory and EBIT experiments [22,24]. Predictions for U^{91+} polarization of the Lyman-α_1 line have been presented. Large differences between calculations with Coulomb, Breit, and Møller potentials have been found. We have verified the accuracy of our e-U^{91+} scattering calculations that include Breit and Møller relativistic corrections by finding good agreement with U^{91+} 1s ionization cross-section measurements of Marrs *et al.* [20] and previous first-order calculations.

With the current extension of the RCCC method we now have a reliable technique for calculating electron scattering on arbitrarily charged ions with an electronic configuration in the first group of the Periodic Table. The reliability is independent of the projectile energy or the transition considered.

ACKNOWLEDGMENTS

The authors would like to thank H. M. Quiney and C. J. Fontes for useful discussions. This work was supported by the Australian Research Council and calculations were performed on the iVEC node of the Australian Partnership for Advanced Computing.

[1] D. V. Fursa and I. Bray, Phys. Rev. Lett. **100**, 113201 (2008).
[2] D. V. Fursa, C. J. Bostock, and I. Bray, Phys. Rev. A **80**, 022717 (2009).
[3] G. Breit, Phys. Rev. **34**, 553 (1929).
[4] G. Breit, Phys. Rev. **36**, 383 (1930).
[5] G. Breit, Phys. Rev. **39**, 616 (1932).
[6] Chr. Møller, Ann. Phys. **406**, 531 (1932).
[7] H. A. Bethe and E. E. Salpeter, *Quantum Mechanics of One- and Two-Electron Atoms* (Springer, New York, 1957).
[8] W. Greiner, *Quantum Electrodynamics* (Springer-Verlag, Berlin, 1996).
[9] J. Sucher, Phys. Rev. A **22**, 348 (1980).
[10] D. W. Walker, J. Phys. B **8**, 760 (1975).
[11] D. Moores and M. Pindzola, J. Phys. B **25**, 4581 (1992).
[12] C. J. Fontes, D. H. Sampson, and H. L. Zhang, Phys. Rev. A **47**, 1009 (1993).
[13] M. S. Pindzola, D. L. Moores, and D. C. Griffin, Phys. Rev. A **40**, 4941 (1989).
[14] M. S. Pindzola, N. R. Badnell, D. L. Moores, and D. C. Griffin, Z. Phys. D: At., Mol. Clusters **21**, S23 (1991).
[15] D. L. Moores and K. J. Reed, Phys. Rev. A **51**, R9 (1995).
[16] D. L. Moores and K. J. Reed, Nucl. Instrum. Methods Phys. Res. B **98**, 122 (1995).
[17] C. J. Fontes, D. H. Sampson, and H. L. Zhang, Phys. Rev. A **51**, R12 (1995).
[18] C. J. Fontes, D. H. Sampson, and H. L. Zhang, Phys. Rev. A **59**, 1329 (1999).
[19] P. Beiersdorfer, Phys. Scr. **T134**, 014010 (2009).
[20] R. E. Marrs, S. R. Elliott, and D. A. Knapp, Phys. Rev. Lett. **72**, 4082 (1994).
[21] *Plasma Polarization Spectroscopy*, Springer Series on Atomic, Optical and Plasma Physics, edited by T. Fujimoto and A. Iwamae (Springer, New York, 2007).
[22] N. Nakamura, D. Kato, N. Miura, T. Nakahara, and S. Ohtani, Phys. Rev. A **63**, 024501 (2001).
[23] K. J. Reed and M. H. Chen, Phys. Rev. A **48**, 3644 (1993).
[24] D. L. Robbins *et al.*, Phys. Rev. A **74**, 022713 (2006).
[25] P. Strange, *Relativistic Quantum Mechanics* (Cambridge University Press, Cambridge, England, 1998).
[26] I. P. Grant and H. M. Quiney, Phys. Rev. A **62**, 022508 (2000).
[27] M. Rose, *Relativistic Electron Theory* (John Wiley and Sons, New York, 1961).
[28] J. Hata and I. P. Grant, J. Phys. B **17**, L107 (1984).
[29] I. P. Grant, Adv. Phys. **19**, 747 (1970).
[30] *Handbook of Mathematical Functions*, edited by M. Abramowitz and I. Stegun (Dover, New York, 1965).
[31] S. A. Napier, D. Cvejanović, J. F. Williams, L. Pravica, D. Fursa, I. Bray, O. Zatsarinny, and K. Bartschat, Phys. Rev. A **79**, 042702 (2009).
[32] M. Maslov, M. J. Brunger, P. J. O. Teubner, O. Zatsarinny, K. Bartschat, D. Fursa, I. Bray, and R. P. McEachran, Phys. Rev. A **77**, 062711 (2008).
[33] W. Kedzierski, A. Abdellatif, J. W. McConkey, K. Bartschat, D. V. Fursa, and I. Bray, J. Phys. B **34**, 3367 (2001).
[34] M. K. Inal and J. Dubau, J. Phys. B **20**, 4221 (1987).
[35] P. Hakel, R. C. Mancini, C. Harris, P. Neill, P. Beiersdorfer, G. Csanak, and H. L. Zhang, Phys. Rev. A **76**, 012716 (2007).
[36] H. L. Zhang, D. H. Sampson, and R. E. H. Clark, Phys. Rev. A **41**, 198 (1990).
[37] G. Weber, GSI Centre for Heavy Ion Research, Darmstadt, Germany (private communication).
[38] I. Bray, Phys. Rev. Lett. **78**, 4721 (1997).
[39] I. E. McCarthy and E. Weigold, *Electron-Atom Collisions* (Cambridge University Press, Cambridge, 1995).